Arab J Sci Eng (2014) 39:7513–7524
DOI 10.1007/s13369-014-1312-3

RESEARCH ARTICLE - CIVIL ENGINEERING

Evaluation of Cyclic Stress–Strain and Liquefaction Behavior of Izmir Sand

Tugba Eskisar · Eyyub Karakan · Selim Altun

Received: 20 September 2013 / Accepted: 30 April 2014 / Published online: 17 August 2014

Abstract This paper presents the results of a series of cyclic triaxial tests carried out on sands with different index properties. Samples from three grain-size distributions of Izmir (Turkey) sand were tested under consolidated-undrained conditions. The tests were performed under two different effective confining pressure values (100 and 200 kPa). The relative densities of the specimens were 30 and 50 %. The results showed that the relative density plays a dominant role in the liquefaction behavior of the sand, whereas the confining pressure increase has greater effects on the stress–strain properties of the sand. It was observed that the relationship between the grain-size diameters and cyclic stress ratios of the sands would be more realistic. It was found that the pore water pressure generation curve falls outside the narrow band proposed by previous studies and a greater coefficient is required for the cycle ratio depending on the soil properties and test conditions. The shear moduli of the sands increased independently of the mean diameter with the relative density under a confining pressure of 100 kPa. Under a confining pressure of 200 kPa, the shear moduli increased with the uniformity coefficient of the sand. Increments in the relative density resulted in a slight increment of the shear moduli for the sands. The goal of the current study was to provide an understanding of the liquefaction and stress–strain behavior of Izmir sand, which represents the material of similar sites with loose alluvial sediments located in earthquake-prone areas found around the world.

T. Eskisar (✉) · S. Altun
Department of Civil Engineering, Ege University, Izmir, Turkey
e-mail: tugba.eskisar@ege.edu.tr

E. Karakan
Department of Civil Engineering, Balikesir University, Balikesir, Turkey

Keywords Liquefaction test · Stress–strain test · Sand · Grain-size distribution

الخلاصة

تعرض هذه الورقة العلمية نتائج سلسلة من الاختبارات الدائرية، ثلاثية المحور التي أجريت على رمال ذات خصائص مؤشر مختلفة. وقد تم اختبار ثلاث عينات توزيعات حجم حبوب من رمال إزمير (تركيا) في ظل ظروف مدمجة -غير مستنزفة. وأجريت الاختبارات تحت قيمتي ضغط حصر فعال مختلفتين (100 كيلو باسكال و 200 كيلو باسكال). وكانت الكثافة النسبية للعينات 30٪ و 50٪، وأظهرت النتائج أن الكثافة النسبية تلعب دورا مهيمنا في سلوك تسييل الرمال، في حين أن لزيادة ضغط الحصر آثاراً أكبر في خصائص الإجهاد والشد من الرمال. وقد لوحظ أن العلاقة بين أقطار حجم الحبوب ونسب الضغوط الدائرية من الرمال سيكون أكثر واقعية. وتبين أن منحنى توليد ضغط مياه المسام يقع خارج النطاق الضيق الذي اقترحته الدراسات السابقة ومطلوب معامل أكبر لنسبة الدورة تبعا لخصائص التربة وظروف الاختبار. و زادت معاملات رجوعية القص من الرمال بشكل مستقل من متوسط القطر مع الكثافة النسبية تحت ضغط حصر من 100 كيلو باسكال. وتحت ضغط من 200 كيلو باسكال حصر زادت معاملات رجوعية القص مع معامل الدمج من الرمال. وأدت الزيادات في الكثافة النسبية إلى زيادة طفيفة في معاملات رجوعية القص للرمال. وكان الهدف من الدراسة الحالية توفير فهم سلوك التسييل والإجهاد ـ الشد من رمال أزمير التي تمثل موادً من مواقع مشابهة مع رواسب غرينية فضفاضة تقع في المناطق المعرضة للزلازل الموجودة في جميع أنحاء العالم.

1 Introduction

The seismic-resistant design of soil structures requires a clear understanding of the soil behavior under earthquake loading. Therefore, it is necessary to consider the ground-shaking characteristics and local site amplifications in estimations of ground response and definitions of structural design loads. Civil engineering projects in Izmir City in Turkey and its vicinity have significantly increased over the last decade

because the population of the city is rapidly increasing. Izmir city is located on deep alluvial sediments capable of amplifying ground motions during an earthquake. Soil layers composed of sand occur frequently and are accompanied by a high groundwater table in the area. For this reason, investigation of the behavior of the Izmir sand has recently received attention.

Izmir is surrounded by 13 active faults [1], and the 1977 ($M_s = 5.3$), 1992 ($M_w = 6.0$), 2003 ($M_d = 5.6$), and 2005 ($M_w = 5.9$) earthquakes are distinctive examples of the many seismic activities that have occurred in the recent past and caused damage in and around Izmir. A rupture along the Izmir fault, which is located along the southern region of the city, will cause large ground deformations and strong ground shaking in Izmir. Additionally, the 1977 earthquake occurred on the Izmir fault. According to the earthquake master plan for Izmir [2], the expected peak ground acceleration for rock sites is between 0.3 and 0.35 g for a 10 % probability of exceedance over 50 years. The plan emphasizes that an earthquake scenario on the Izmir fault with a magnitude of $M_s = 6.5$ is expected. The combination of local soil properties and moderate-high seismic activity makes it vitally important to characterize the dynamic strength and liquefaction behavior of soils under cyclic loading. Areas with active seismicity and similar geological conditions are present worldwide in such locations as Christchurch (New Zealand), Ohio (USA), and Taipei (Taiwan) [3–5]. Therefore, the findings of this study not only constitute an example at the international level but also contribute to an understanding of the dynamic behavior sands under similar conditions.

Early studies of liquefaction were mostly devoted to clean sands [6]. The present state of the art of liquefaction of sands has progressed to a stage at which reasonable estimates of the liquefaction potential can be produced based on laboratory testing or on in-situ test data [7–10].

The undrained response of coarse-grained soils to cyclic loading, which may be induced by an earthquake, has received increased attention after several liquefaction-induced failures were observed to occur with the associated detrimental effects. The vital role of excess pore water pressure in reducing effective stress, inducing excessive strains, and consequently causing liquefaction cannot be ignored. From the 1960s up to the present, several researchers have examined the fundamental aspects of cyclic liquefaction or strain-softening behavior for granular and sandy soils [11–14]. The maximum dynamic shear modulus and damping ratio are descriptive soil parameters for many geotechnical earthquake engineering applications that involve many types of loading and many potential mechanisms of failure, not only at low strains but also at intermediate and high strains. For problems dominated by wave propagation effects, only low levels of strains are induced in the soil, and for problems involving the stability of masses of soil, large strains are induced in the soil [15]. In recent years, selected studies were performed to investigate the behavior of soils at small strain levels, and estimations of the dynamic shear modulus and damping ratio for different types of soils were also examined [16–18].

This paper presents a systematic experimental investigation with three different grain-size distributions of Izmir sand using a cyclic triaxial device. The main objective was to explore (1) the liquefaction and stress–strain behavior of sands with relative densities of 30 and 50 % under consolidated-undrained conditions with the effective confining stress values of 100 and 200 kPa; (2) the pore water pressure development, its relationship with effective stress, and its comparison with the conventional models; and (3) the effects of gradation parameters (mean grain size and uniformity coefficient) on the cyclic resistance and the dynamic properties of the sands at small strain levels.

2 Materials and Experimental Program

Local sand is obtained from the city center of Izmir in Turkey. The sand is classified as poorly graded sand (SP) according to the Unified Soil Classification System. Coarse-grained sand and fine-grained sand are obtained by sieving the original soil mass. The sand portions consisting of grain sizes between no. 4 and no. 30 sieves and no. 60 and no. 200 sieves are separated in this manner. The index properties of the sands are presented in Table 1. In this study, the coarse sand, original sand, and fine sand are denoted as CS, OS, and FS, respectively.

An experimental program was prepared to investigate the influence of the grain-size distribution curves of sand on

Table 1 Index properties of the sand with three different gradations

	Coarse sand (CS)	Original sand (OS)	Fine sand (FS)
USCS[a] symbol	SP	SP	SP
d_{10} (mm)	0.52	0.15	0.11
d_{30} (mm)	0.74	0.28	0.17
d_{50} (mm)	1.25	0.53	0.23
d_{60} (mm)	1.50	0.70	0.26
Coefficient of uniformity, C_u	2.88	4.67	2.36
Coefficient of curvature, C_c	0.70	0.75	1.01
Maximum void ratio, e^b_{max}	0.92	0.84	1.09
Minimum void ratio, e^c_{min}	0.67	0.56	0.79
Specific gravity, G^d_s	2.66	2.67	2.69

[a] USCS = Unified Soil Classification System, [b] ASTM D4253, [c] ASTM D4254, [d] ASTM D854

Table 2 Cyclic testing program of the study

Poorly graded (SP) sand				
Confining pressure (kPa)	100	100	200	200
Relative density (%)	30	50	30	50
Coarse sand (SP sand between no. 4 and no. 30 sieves)				
Confining pressure (kPa)	100	100	200	200
Relative density (%)	30	50	30	50
Fine sand (SP sand between no. 60 and no. 200 sieves)				
Confining pressure (kPa)	100	100	200	200
Relative density (%)	30	50	30	50

the stress–strain parameters (Table 2), and twelve cyclic test cases are shown in Table 2. The test cases are combinations of grain-size distribution and relative density of the sand and the confining pressure experienced by the soil sample. Five cyclic triaxial tests are performed in each test case. In addition to the routine experimental program, certain randomly selected test cases are rerun to check the validation of sample preparations of similar density and loading conditions to verify the repeatability and the accuracy of the results. The experiments are conducted on specimens with a diameter of 50 mm and a height of 100 mm. The specimens are prepared using the method of air pluviation with a controlled flow rate and constant fall height for a calculated amount of dried sand (JGS 0520-2000 [19]) and are subsequently tested according to JGS 0541-2000 [20]. JGS (Japanese Geotechnical Society) standards are preferred as they are based on the concept that the cyclic deformation properties of geomaterials are allowed to be measured in triaxial test using a single specimen over a wide strain range from 10^{-6} to 10^{-2}. The specimens are flooded with carbon dioxide followed by de-aired water, and back pressure is applied to saturate the specimens. Skempton's pore water pressure value ($B = u/\Delta\sigma$) is verified to vary between 0.96 and 1.00. The specimens are isotropically consolidated to the desired effective stress, and stress-controlled undrained cyclic loading is subsequently applied. In the liquefaction tests, the loading sequence applies a certain number of cycles necessary to reach a specified level of cyclic stress under a frequency of 0.1 Hz until the specimen develops a double-amplitude axial strain (ε_{DA}) of 5 %.

During cyclic loading, continuous records are obtained for the excess pore water pressure (Δu), cyclic axial strain (ε_c), and the cyclic deviator stress ratio applied to the specimen. Following the recommendations of JGS 0541-2000 [20], two criteria are considered to define liquefaction. If the amplitude of cyclic axial load is relatively large, the number of cycles needed to cause liquefaction is accepted as the number of cycles needed to reach a maximum value of excess pore water pressure equal to 95 % of the effective confining stress; otherwise, it is recognized as the number of cycles needed to reach a double amplitude of 5 % of the axial displacement of the specimen. The experiments progress until all specimens reach 10 % of the axial displacement. Typical test results obtained from a cyclic triaxial test conducted on OS sand with a relative density of 30 % and subjected to an effective confining pressure of 100 kPa are illustrated in Fig. 1.

The cyclic deviator stress applied to the specimen with a given number of cycles is presented in Fig. 1a. Two-way cyclic loading, which involves a continuous sequence of compression and extension, was regularly applied to simulate dynamic conditions. Figure 1b shows the variation of the corresponding cyclic axial strain with the number of cycles. At the beginning of the test, the loading and strains move on the same axis, but as the number of cycles increases, the strains became more dominant on the compression side. The variation of pore water pressure with the number of loading cycles is shown in Fig. 1c. The progress of the pore water pressure ratio with the number of cycles follows a steady trend. After 60 cycles, the pore water pressure ratio exceeds 95 %, and this condition stimulates the cyclic axial strains to vary considerably over a wider range. The plot of the pore water pressure ratio with cyclic axial strain, the deviator stress with cyclic axial strain, and the effective stress path are shown in Fig. 1d–f, respectively. In Fig. 1d, when the pore water pressure ratio reaches 80 %, the cyclic axial strain is approximately 0.5 %. Further development of the pore water pressure results in +5.5 and −3.5 % strain levels for a total strain of 9 %. Figure 1e indicates the occurrence of small axial strain (approximately 0.5 %) before initial liquefaction and a nearly 5 % double-amplitude strain at 67 cycles of loading. However, once the initial liquefaction is triggered, the specimen rapidly experiences large strains, within approximately one loading cycle, and subsequently fails due to softening of the soil, which is the characteristic of contractive behavior of loose sand due to the pore water pressure build up. In Fig. 1f, it should be noted that the stress path is directed to the compression side relative to the trend of cyclic axial strain. At the end of this test case, necking occurred in the specimen because of the flexible boundary in the vertical direction, and this condition accelerated the non-uniform stress and deformation in the specimen at the end of liquefaction.

To determine the stress–strain characteristics of the sand, a series of tests are performed in this study. The same cases as in the liquefaction tests are examined in the deformation tests. In the undrained cyclic test, a total of eleven cyclic loadings are imposed on the specimen using a single amplitude cyclic axial strain of less than 0.001 % [21]. During the experiments in this study, the cyclic loading is applied via an axial load in a controlled manner for a sinusoidal load at a constant frequency of 0.1 Hz for all test cases. After the end of each cyclic loading, drainage is allowed, and the change in height and volume of the specimen is recorded. The rate of

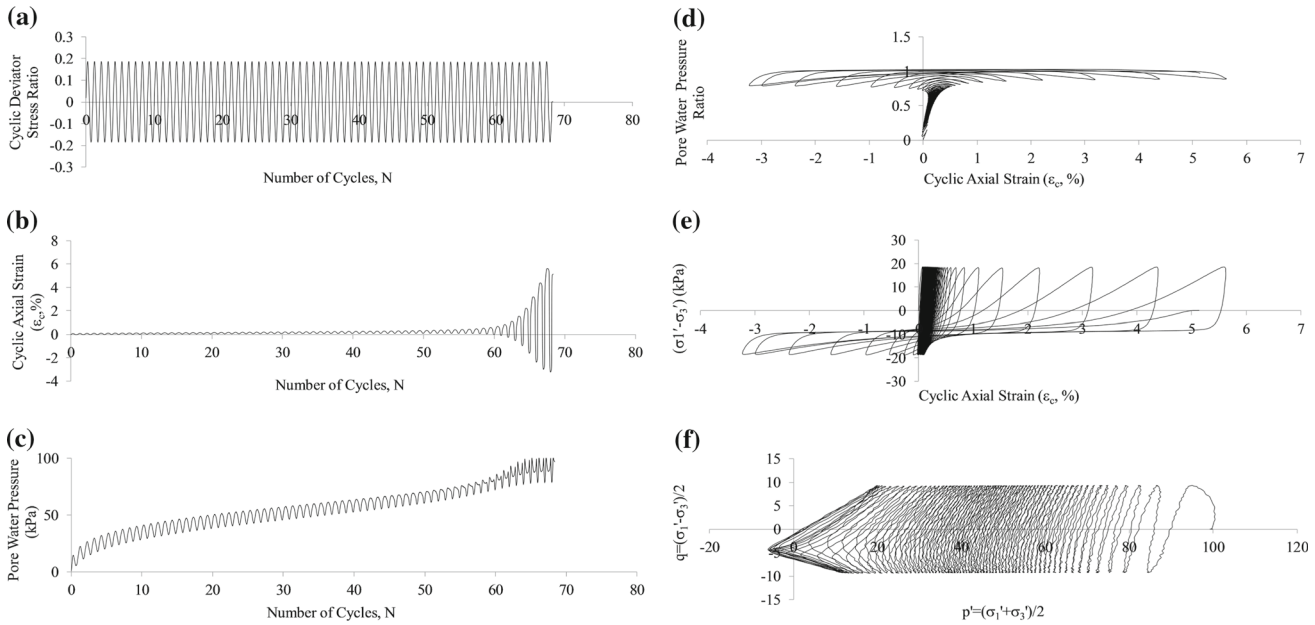

Fig. 1 **a** Variation of cyclic stress ratio, **b** cyclic axial strain and **c** pore water pressure with loading cycles, **d** power water pressure ratio with cyclic axial strain, **e** deviator stress with cyclic axial strain, and **f** stress path for a sand specimen ($D_r = 30\,\%$, $\sigma'_0 = 100\,\text{kPa}$)

axial strain at the end of each consolidation stage is ensured to be less than 0.01 %/min, and the drainage is closed. Twice the amount of cyclic loading is applied in every step until it is impossible to continue within the limitations of the test device. The total number of data points for each quantity required to form a single hysteresis loop is more than forty in every deformation test. Typical test results obtained from undrained cyclic triaxial tests performed by following JGS 0542-2000 [21] are presented in Fig. 2a–d for the same specimen conditions as in Fig. 1.

In Fig. 2a, 75 loading stages are included in the deformation test. The pore water pressure is dissipated at the end of each loading; therefore, a pore water pressure ratio of 1.0 could not be obtained. The negative values of the pore water pressure ratio denote the condition of drainage allowance at the end of the loading stages. Because the deviator stress level is limited, the test progressed to a compression pressure of 250 kPa, as shown in Fig. 2b. The total axial strain of this specimen reached 0.7 % (Fig. 2c). Although a deviator stress of 250 kPa corresponds to an axial strain of 0.4 % on the compression side, a deviator stress of 130 kPa corresponds to an axial strain of 0.3 % in the extension side at the end of the test (Fig. 2d).

3 Evaluation of Test Results and Discussion

The testing program for the specimens in the cyclic triaxial test device is described in Table 2. During this program, the results of several test cases were obtained, and the liquefaction and stress–strain behaviors of the specimens were evaluated by means of relative density, double amplitude of axial strain, pore water pressure development, and the effect of grain size.

3.1 Effect of Relative Density and Confining Pressure on the Cyclic Stress

Cyclic stresses are plotted versus the number of cycles for the results of cyclic triaxial tests performed on saturated samples of coarse, original, and fine sands (Fig. 3a–f).

The curves in Fig. 3 are achieved for relative density values of 30 and 50 % under constant confining pressures of 100 and 200 kPa. Similar curves are achieved for the 5 and 10 % double-amplitude axial strains that confirm the cyclic stress versus number of cycles relationships for three types of sand. The curves for three types of sand follows the order of $D_r = 50\,\% - \sigma'_0 = 200\,\text{kPa}$, $D_r = 30\,\% - \sigma'_0 = 200\,\text{kPa}$, $D_r = 50\,\% - \sigma'_0 = 100\,\text{kPa}$, and $D_r = 30\,\% - \sigma'_0 = 100\,\text{kPa}$ from the upper to lower range. The effect of relative density change is more pronounced than that of the effective stress change in Fig. 3a–d. This observation also could be related to the grain-size distributions of CS and OS types of sand. The gradation curves of these sands are quite similar, and the coefficient of curvature is the closest parameter among the other gradation parameters given in Table 1.

The FS sand has a different grain-size distribution than that of CS and OS, and its grain-size distribution lies in a narrower range. Hence, the effect of relative density is not as prevalent as that shown in Fig. 3e, f. This type of sand is more sensitive to the change of effective stresses because the curves of

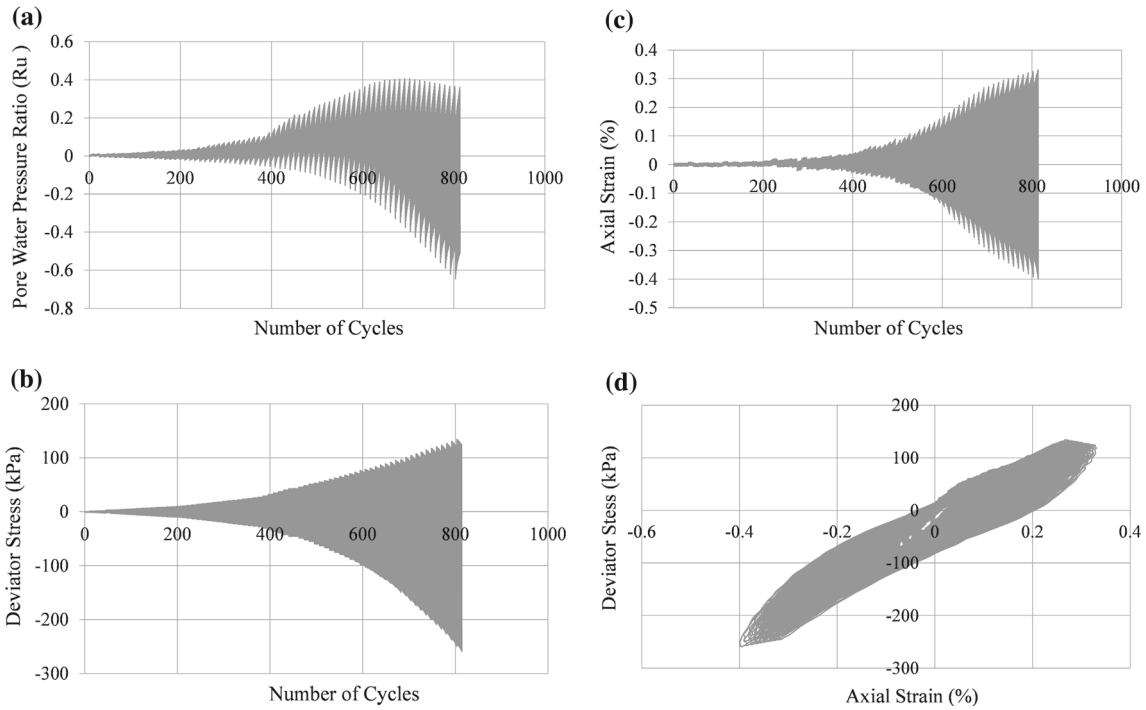

Fig. 2 **a** Variation of pore water pressure ratio, **b** deviator stress, and **c** axial strain with loading cycles; **d** relationship of deviator stress with axial strain for a sand specimen ($D_r = 30\,\%$, $\sigma'_0 = 100\,\text{kPa}$)

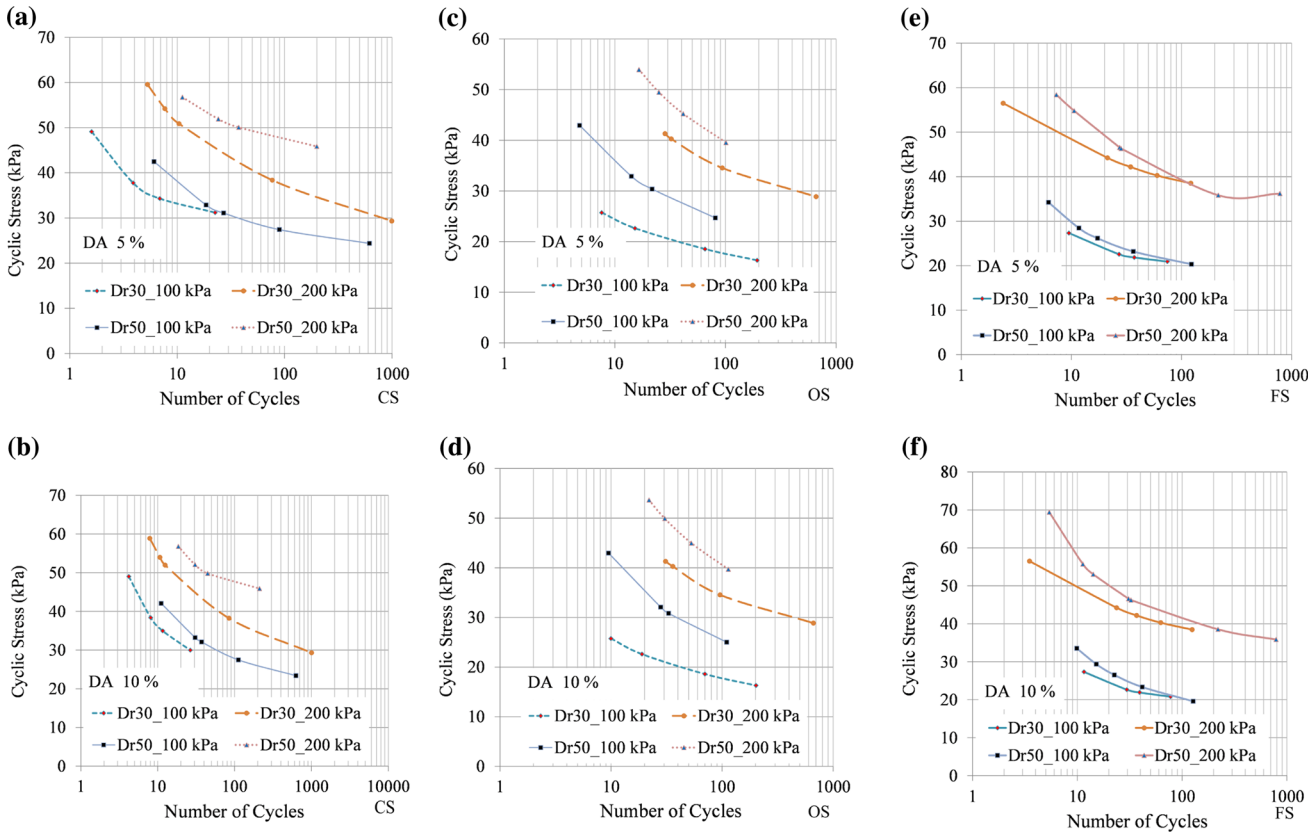

Fig. 3 Liquefaction resistance of CS, OS, and FS sands for a double amplitude of axial strain of 5 % (**a**, **c**, **e**) and 10 % (**b**, **d**, **f**), respectively

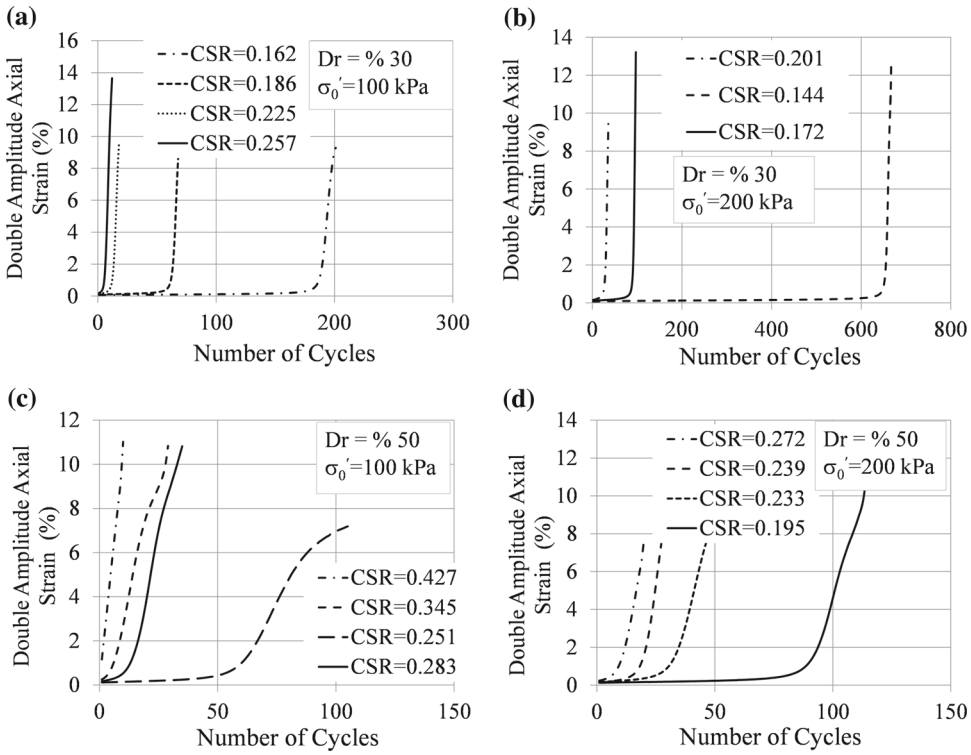

Fig. 4 Variation of double-amplitude axial strain with number of loading cycles for OS sand: **a** $D_r = 30\,\%$ and $\sigma_0' = 100\,\text{kPa}$, **b** $D_r = 30\,\%$ and $\sigma_0' = 200\,\text{kPa}$, **c** $D_r = 50\,\%$ and $\sigma_0' = 100\,\text{kPa}$, and **d** $D_r = 50\,\%$ and $\sigma_0' = 200\,\text{kPa}$

the same confining pressures nearly overlap with each other. These data indicate that larger cyclic stresses are generated at 200 kPa than at 100 kPa, particularly at a lower number of cycles. The cyclic stresses are effectively dependent on confining pressure, with higher cyclic stresses obtained at higher effective confining pressures. This condition is valid for specimens with relative densities of both 30 and 50 %.

3.2 Effect of Double Amplitude (DA) of Axial Strain

The changes in the double-amplitude axial strain with the number of cycles under each testing condition are shown in Fig. 4a–d with the corresponding cyclic stress ratios (CSR). Liquefaction occurred instantly in OS specimens with lower relative densities because the double amplitude of axial strain follows a perpendicular path (Fig. 4a, b). For medium density specimens of OS sand, the deformation increases gradually with the number of cycles over which the double amplitude of strain develops in time (Fig. 4c, d). Similar observations are valid for CS and FS sands, and therefore, they are not discussed in further detail.

3.3 Effect of Grading Characteristics on Liquefaction Resistance

The gradation parameters are evaluated in terms of d_{10}, d_{30}, d_{50} (mean diameter), d_{60}, coefficient of uniformity (C_u), and coefficient of curvature (C_c) accompanied by the cyclic stress ratios (CSR) for 15 cycles of uniform loading. A relationship between C_u or C_c and the CSR was not observed for different test conditions. The cyclic resistance decreased consistently with the grain size (Fig. 5). This observation is in agreement with the findings of Miura et al. [22]. Polito [23] reported that the cyclic resistance increases as the mean diameter increases for clean sands. It is observed that the relationship is more prominent between the grain-size diameters and CSR.

3.4 Effect of Pore Water Pressure Development

The pore water pressure builds up gradually during the liquefaction tests and reaches the initially applied confining stress; this buildup of pore water pressure generation depends on the magnitude of cyclic stress ratio (CSR) as well as the density of the soil. In addition, the effect of the number of loading cycles on the magnitude of pore water pressure is essentially a function of the shear strain [24].

A number of studies exist that aim at assessment of the pore water pressure response of fully saturated clean sands. Marcuson et al. [25] used the pore water pressure ratio to estimate the reduction of soil stiffness during earthquake loading. Oda et al. [26] linked the increment in pore water pressure at the end of the first cycle to the number of cycles required to cause a double-amplitude axial strain of 5 % in cyclic triaxial tests, regardless of relative density and cyclic shear ratio. Dobry [27] proposed upper and lower boundaries in the pore water pressure ratio versus shear strain

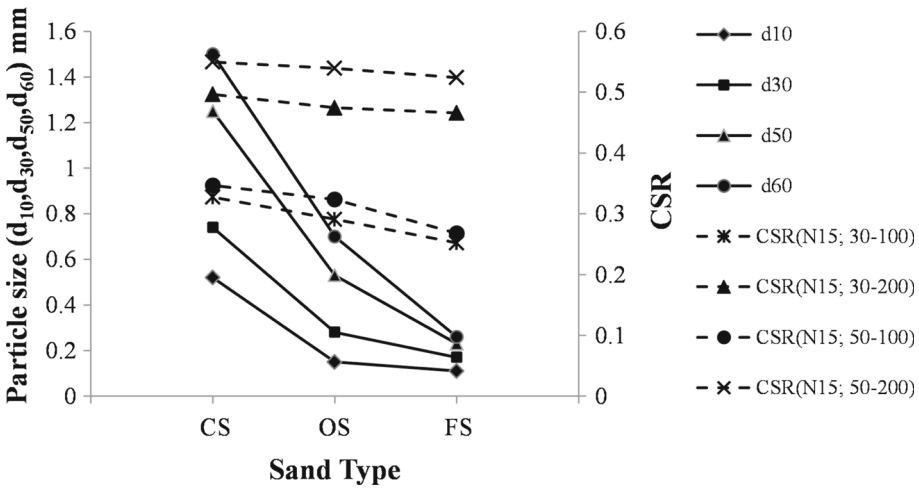

Fig. 5 Variation of the cyclic stress ratio with the grain sizes of sands used in this study

domain based on the results of strain-controlled cyclic tests on poorly graded sands, and these boundaries are presented in Fig. 6. A major disagreement exists in the pore water pressure ratio versus the axial shear strain responses of stress and strain-controlled test data because of the significantly different strain paths followed during these cyclic tests. In simpler terms, the boundary curves of Dobry [27] correspond to a specific case in which ten cycles of shear strains were applied, and the corollary pore water pressure ratio values were estimated at the end. However, during stress-controlled cyclic testing, the estimated pore water pressure ratio values correspond to the first occurrence of the recorded maximum strain levels and are less dependent on the stress histories. To compare the boundary curves of Dobry [27] with those of this study, pore water pressure values corresponding to the double amplitude of axial strain levels of 5 % are obtained and used to graph the data of Fig. 6a–c.

The CS sand is located near the lower boundary of the curve offered by Dobry [27], as shown in Fig. 6a. The OS sand remains slightly below the lower boundary of the curve (Fig. 6b), and the FS sand lies exactly between the upper and lower boundaries of the proposed curves of Dobry [27] (Fig. 6c). If the average shear strain levels are considered for a constant pore water pressure, the order of shear strain levels shows an increase from fine sand to coarse sand. For example, if the pore water pressure is taken as 0.4, the average shear strains of fine, original, and coarse sands are 0.1, 0.2, and 0.4 %, respectively. This trend proceeds until the pore water pressures reach 0.95, and high levels of shear strains are achieved thereafter. For a constant level of shear strain, the pore water pressures increase from coarse to fine sand. For instance, if the shear strain is taken as 0.1 %, the pore water pressure values of the sands are 0.45 for coarse sand, 0.51 for original sand, and 0.58 for fine sand. This sequence is in agreement with the median grain size of the sand types (d_{50} of 0.23, 0.53, and 1.25 mm) used in this study. The pore water pressure change is associated with grain size, especially the mean diameter of sand [28,29]. The test results reveal that for sands with different gradation, the one that has a smaller mean grain size (d_{50}) is more susceptible to liquefaction.

Another comparison is carried out by obtaining the cycle number ratios for which the pore water pressure ratio is 1. Lee and Albaisa [30] recommended upper and lower boundaries for residual pore water pressure ratios for Monterey and Sacramento sands, whereas El Hosri et al. [31] proposed curves for silty clays. Seed et al. [32] developed an empirical model for predicting the rate of pore water pressure using data from tests performed on clean sands. The boundaries presented by the aforementioned authors are shown in comparison with the results of this study in Fig. 7a–c. Variation of the pore water pressure ratio versus the cycle number ratio of OS sand constitutes the upper boundary curve that covers the model curves offered by El Hosri et al. [31], and the lower boundary of OS sand overlaps with upper boundary curves of Lee and Albaisa [30] and Seed et al. [32] (Fig. 7a). The CS sand lies between the lower boundary of El Hosri et al. [31] and the upper boundary curves of Lee and Albaisa [30] and Seed et al. [32] (Fig. 7b). The FS sand shows the largest variation, and the curves of this type of sand proceed slightly over the curves of El Hosri et al. [31] and somewhat lower than the upper boundary offered by Seed et al. [32] (Fig. 7c). The built-up pore water pressure is much faster at the beginning of loading until it reaches 40 %, and this value corresponds to a cycle number ratio of 0.1 in all tests; subsequently, the rate of increment of the pore water pressure slows.

The model proposed by Seed et al. [32] can be stated in a closed-form solution in Eq. (1)

$$r_u = \frac{1}{2} + \frac{1}{\pi}\sin^{-1}\left[2\left(\frac{N}{N_L}\right)^{1/\propto} - 1\right] \quad (1)$$

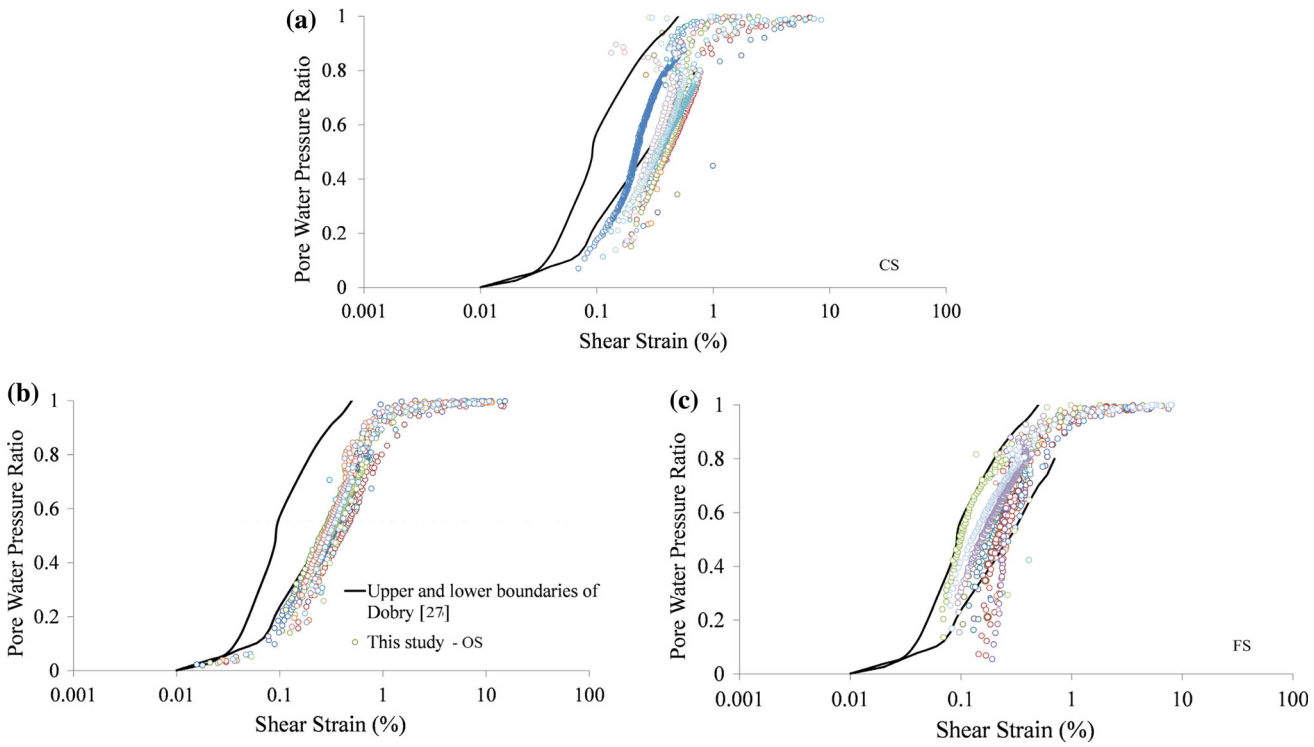

Fig. 6 Comparison of the test results of **a** CS sand **b** OS sand, and **c** FS sand with boundary curves of Dobry [27]

where it is recommended that α should be stated as a function of the soil properties and test conditions (the average is reported as 0.7), N is the number of equivalent uniform loading cycles, and N_L is the number of cycles required to produce initial liquefaction ($r_u = 1.0$).

Later studies benefitted from this approach to predicting pore water pressure response and reported that the pore water pressure generation curve falls outside the narrow band proposed by Seed et al. [33] and that the α coefficient results in a lower bound of the predicted generated pore water pressures rather than an average [34].

To find the estimates of the α coefficient for the sands of this study, a third-degree polynomial function is fit between the pore water pressure ratios (r_u) and cycle ratios (N/N_L). By performing multiple regression analysis, the coefficients of the polynomial equations are calculated for the condition of $0 < r_u < 1$ and given in Table 3. After obtaining a model equation for each type of sand, the α coefficient for each sand type is obtained. The α coefficients for three types of sand are given as 2.1 for CS and OS sands and 2.4 for FS sand.

3.5 Effect of Grain-Size Distribution on Dynamic Shear Modulus and Damping Ratio

The measured shear modulus and damping ratio curves for CS, OS, and FS sands are given in Fig. 8a–d as a function of relative density and for different confining pressures. For tests with $D_r = 30\,\%$ and $\sigma'_0 = 100\,\text{kPa}$, the maximum shear modulus, G_{max}, is approximately 110 MPa. When the confining pressure increases to $\sigma'_0 = 200\,\text{kPa}$, the shear modulus is 170 MPa for CS and FS and 180 MPa for OS sand. For specimens with $D_r = 50\,\%$ and $\sigma'_0 = 100\,\text{kPa}$, the CS, FS, and OS sands have shear moduli of 120, 100, and 140 MPa, respectively. When σ'_0 is 200 kPa, the CS, FS, and OS sands are sorted as 190, 180, and 220 MPa.

Iwasaki and Tatsuoka [17] reported that for a constant void ratio, the maximum shear modulus is strongly affected by the grain-size distribution curve. In their study of poorly graded sands ($C_u < 1.8, 0.16 < d_{50} < 3.2\,\text{mm}$) without fines content, the values of maximum shear modulus were found to be independent of d_{50}. Menq and Stokoe [35] performed RC tests on specimens of natural river sand without fines content. In contrast to the work of Iwasaki and Tatsuoka [17], Menq and Stokoe [35] reported a slight increase of the maximum shear modulus with increasing d_{50} for a constant void ratio and confining pressure. Additionally, steeper curves of G_{max} were obtained for the coarse material. These researchers found that for a constant relative density, the maximum shear modulus increases with the coefficient of uniformity. Edil and Luh [36] proposed a relationship for the maximum shear modulus for a confining pressure of 211 kPa. In this relationship, the maximum shear modulus increased with decreasing void ratio for fine sands.

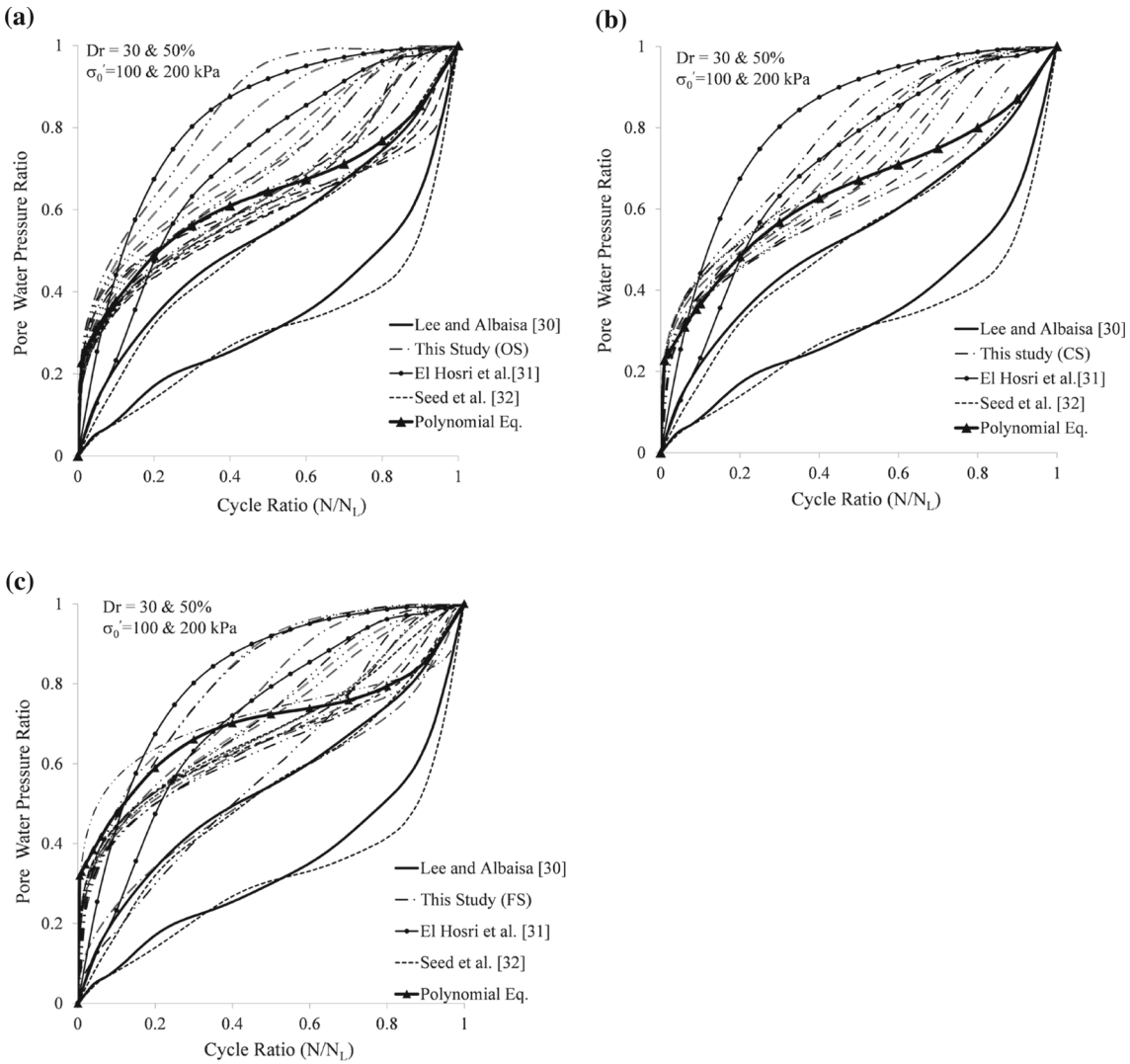

Fig. 7 Pore water pressure generation curves of three sands compared with the models of Lee and Albaisa [30], El Hosri et al. [31], and Seed et al. [32]

Table 3 Regression analysis of three sands and estimates of α coefficients

Sand type	Data points	X_0	X_1	X_2	X_3	R^2	α
OS	1,511	0.22	1.85	−2.92	1.83	0.857	2.1
CS	1,678	0.21	1.81	−2.50	1.45	0.918	2.1
FS	2,127	0.31	1.97	−3.25	1.93	0.815	2.4

In this study, for a confining pressure of 100 kPa, the maximum shear modulus increases with relative density independent of d_{50}. For a confining pressure of 200 kPa, the maximum shear modulus increases with the coefficient of uniformity, and the highest maximum shear modulus value is measured in OS sand in which the coefficient of uniformity has a maximum value compared with the other types of sand. Similar to the conclusion of Edil and Luh [36], the increment of relative density results a slight increment of the maximum shear modulus of the sands.

The observed damping ratio curves are rather independent of the mean grain size and coefficient of uniformity (Fig. 8). For loose sand specimens ($D_r = 30\,\%$), the highest damping ratio is observed in FS sand, and for medium dense specimens ($D_r = 50\,\%$), the lowest damping ratio is observed in FS sand.

4 Conclusions

An extensive series of experiments was carried out via cyclic triaxial tests on sands with different index properties obtained from Izmir, an earthquake-prone area in Turkey. The liquefaction and stress–strain behavior of the sands were investigated in laboratory triaxial tests performed on reconstituted specimens. Three different grain-size distributions

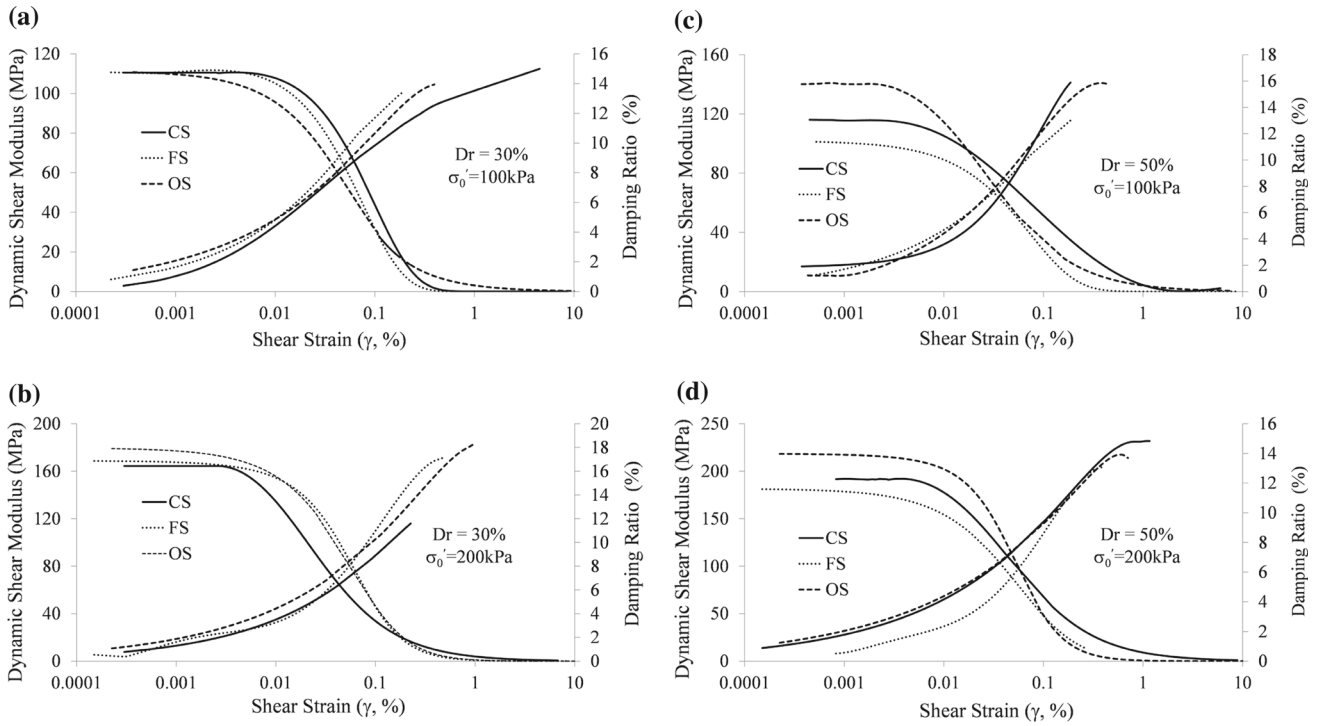

Fig. 8 Variation of dynamic shear modulus and hysteretic damping ratio with shear strain for three sands in the test cases of **a** $D_r = 30\,\%$ and $\sigma_0' = 100\,\text{kPa}$, **b** $D_r = 30\,\%$ and $\sigma_0' = 200\,\text{kPa}$, **c** $D_r = 50\,\%$ and $\sigma_0' = 100\,\text{kPa}$, and **d** $D_r = 50\,\%$ and $\sigma_0' = 200\,\text{kPa}$

were considered. Loose ($D_r = 30\,\%$) and medium dense ($D_r = 50\,\%$) specimens were consolidated under confining pressures of 100 and 200 kPa. A total of 48 successful cyclic tests and 12 deformation tests were performed with these combinations of relative density and effective confining pressures.

The principle conclusions drawn by this paper are as follows:

- The curves for three types of sand follow the order of $D_r = 50\,\% - \sigma_0' = 200\,\text{kPa}$, $D_r = 30\,\% - \sigma_0' = 200\,\text{kPa}$, $D_r = 50\,\% - \sigma_0' = 100\,\text{kPa}$, and $D_r = 30\,\% - \sigma_0' = 100\,\text{kPa}$ cases from the upper to lower range. The effect of relative density change is more pronounced than the effective stress change. If the number of cycles corresponding to the initial liquefaction of CS and OS sands is observed, the increment of the relative density is proportional to the cyclic stresses experienced by the specimens. However, the fine sand data indicate that larger cyclic stresses are generated at 200 kPa than at 100 kPa, particularly at lower numbers of cycles. It is observed that the cyclic stresses are dependent on the effective confining pressure, with higher cyclic stresses obtained at higher effective confining pressures. It is concluded that CS and OS sands are more sensitive to changes in relative density, whereas FS sand is affected by effective stresses.
- By considering three types of sand under different relative densities and confining pressures, it is observed that the predominant relationship exists with different grain sizes of sand rather the uniformity coefficient and coefficient of curvature. The cyclic resistance decreased accordingly with grain size, which is in agreement with the findings of Miura et al. [22] and Polito [23]. A further evaluation of the cyclic resistance and grain sizes of different types of natural sands may enable the development of a numerical relationship in the future studies.
- The double-amplitude axial strain development is more rapid in samples with lower relative density.
- If average shear strain levels are considered for a constant pore water pressure, the order of shear strain levels shows an increase from fine sand to coarse sand. For a constant level of shear strain, the pore water pressures increases from coarse to fine sand. The pore water pressure development level in the second condition reveals that for sands with different gradation, the one with a smaller mean grain size (d_{50}) is more susceptible to liquefaction.
- The pore water pressure development with the cycle ratio for three types of sand falls between the upper limit of El Hosri et al. [31] and lower limit of Seed et al. [32]. The pore water pressure ratio development curves are evaluated for all sand types and the α coefficient of Seed's

equation is suggested as 2.1 for coarse sand and 2.4 for fine sand.

- The increment in effective stress results in an increment of shear modulus for a given strain level for specimens with the same relative density.
- In this study, for a confining pressure of 100 kPa, the maximum shear modulus increases with relative density independent of d_{50}. For a confining pressure of 200 kPa, the maximum shear modulus increases with the coefficient of uniformity, and the highest maximum shear modulus value is measured in OS sand in which the coefficient of uniformity takes on a maximum value compared with the other types of sand. Similar to the conclusion of Edil and Luh [36], the increment of relative density results in a slight increment of the maximum shear modulus of the sands.
- Damping ratios were not found to be related to the gradation of the sand.

Both relative density and effective confining pressure are important parameters required to evaluate the cyclic behavior of sandy soils. However, in this study, it is observed that relative density is more dominant on the liquefaction behavior of the sand, whereas the confining pressure increase has a greater effect on the stress–strain properties of the sand.

References

1. Emre, Ö.; Özalp, S.; Doğan, A.; Özaksoy, V.; Yıldırım, C.; Göktaş, F.: Active Faults of İzmir and Their Earthquake Potentials, p. 86. MTA Report No: 10754 (in Turkish) (2005)
2. Erdik, et al.: İzmir Deprem Senaryosu ve Deprem Master Planı. http://www.İzmir.bel.tr/İzmirdeprem/İzmirrapor.htm (in Turkish) (1999)
3. Bobet, A.; Salgado, R.; Loukidis, D.: Seismic Design of Deep Foundations. Publication FHWA/IN/ JTRP-2000/22. Joint Transportation Research Program, Indiana Department of Transportation and Purdue University, West Lafayette, Indiana (2001)
4. Cubrinovski, M.; Pampanin, S.; Bradley, B.: Geotechnical and structural aspects of the 2010–2011 Christchurch (New Zealand) earthquakes. In: Garevski, M. (ed.) Earthquakes and Health Monitoring of Civil Structures, pp. 1–35. Springer, Dordrecht (2013)
5. Chang, M.; Kuo, C.; Hsu, R.; Shau, S.; Lin, T.: Liquefaction potential and post-liquefaction settlement evaluations of the Chuoshui River alluvial fan in Taiwan. Bull. Eng. Geol. Environ. **71**(2), 325–336 (2013)
6. Seed, H.B.; Lee, K.L.: Studies of liquefaction of sands under cyclic loading conditions. In: Report TE-65, Department of Civil Engineering. University of California, Berkeley (1965)
7. Youd, T.L.; Idriss, I.M.: Liquefaction resistance of soils: summary report from the 1996 NCEER and 1998 NCEER/NSF workshops on evaluation of liquefaction resistance of soils. J. Geotech. Geoenviron. Eng. ASCE **127**(4), 297–313 (2001)
8. Youd, T.L.; Idriss, I.M.; Andurus, R.D.; Arango, I.; Castro, G.; Christian, J.T.; Dobry, R.; finn, W.D.L.; Harder, L.F.; Haymes, M.E.; Ishihara, K.; Koester, J.P.; Liao, S.S.C.; Marcusson, W.F.; Martin, G.R.; Mitchell, J.K.; Moriwaki, Y.; Power, M.C.; Robertson, P.K.; Seed, R.B.; Stokoe, K.H.: Liquefaction resistance of soils: summary report from the 1996 NCEER and 1998 NCEER/NSF workshops on evaluation of liquefaction resistance of soils. J. Geotech. Geoenviron. Eng. ASCE **127**(10), 817–833 (2001)
9. Idriss, R.M.; Boulanger, R.W.: Soil Liquefaction During Earthquakes, p. 243. Report No. MNO-12, Earthquake Engineering Research Institute, California (2008)
10. Chang, W.J.; Rathje, E.M.; Stokoe, K.H.; Hazirbaba, K.: In situ pore pressure generation behaviour of liquefiable sand. J. Geotech. Geoenviron. Eng. ASCE **133**(8), 921–931 (2007)
11. Seed, H.B.; Lee, K.L.: Liquefaction of saturated sands during cyclic loading. J. Soil Mech. Found. Div. **92**(6), 105–134 (1966)
12. Ishihara, K.: Stability of natural deposits during earthquakes. In: Proceedings of 11th International Conference on Soil Mechanics and Foundation Engineering, San Francisco, CA, A. A. Balkema, Rotterdam, pp. 321–376 (1985)
13. Žlender, B.; Trauner, L.: The dynamic properties of the snail soil from the Ljubljana Marsh. Acta Geotechn. Slov. **4**(2), 49–61 (2007)
14. Towhata, I.: Geotechnical Earthquake Engineering. Springer, Berlin (2008)
15. Kramer, S.L.: Geotechnical Earthquake Engineering. pp. 653 Prentice Hall, New Jersey (2008)
16. Hardin, B.O.; Black, W.L.: Closure to vibration modulus of normally consolidated clays. J. Soil Mech. Found. Div. ASCE **95**(SM6), 1531–1537 (1969)
17. Iwasaki, T.; Tatsuoka, F.: Effects of grain size and grading on dynamic shear moduli of sands. Soils Found. **17**(3), 19–35 (1977)
18. Marcuson, W.F.; Wahls, H.E.: Time effects on dynamic shear modulus of clays. J. Solid Mech. Found. Div. ASCE **98**(12), 1359–1373 (1972)
19. JGS 0520-2000. Preparation of Soil Specimens for Triaxial Tests. Japanese Geotechnical Society (in English)
20. JGS 0541-2000. Method for Cyclic Undrained Triaxial Tests on Soils. Japanese Geotechnical Society (in English)
21. JGS 0542-2000. Method for Cyclic Triaxial Test to Determine Deformation Properties of Geomaterials. Japanese Geotechnical Society (in English)
22. Miura, S.; Toki, S.; Tatsuoka, F.: Cyclic undrained triaxial behavior of sand by a cooperative test program in Japan. In: Ebelhar, R.J.; Drenvich, V.P.; Kutter, B.L. (eds.) Dynamic Geotechnical Testing II. ASTM STP, vol. 1213, pp. 246–260. American Society for Testing and Materials (ASTM), Philadelphia (1994)
23. Polito, C.P.: The Effects of Non-Plastic and Plastic Fines on the Liquefaction of Sandy Soils. PhD. Thesis, Virginia Polytechnic Institute and State University, Virginia (1999)
24. Erten, D.; Maher, M.H.: Cyclic undrained behavior of silty sand. Soil Dyn. Earthq. Eng. **14**, 115–123 (1995)
25. Marcuson, W.F.; Hynes, M.E.; Franklin, A.G.: Evaluation and use of residual strength in seismic safety analysis of embankments. Earthq. Spectra **6**(3), 529–572 (1990)
26. Oda, M.; Kawamoto, K.; Suzuki, K.; Fujimori, H.; Sato, M.: Microstructural interpretation on reliquefaction of saturated granular soils under cyclic loading. J. Geotech. Geoenviron. Eng. **127**(5), 416–423 (2001)
27. Dobry, R.: Liquefaction of Soils During Earthquakes. Report No. CETS-EE-001, National Research Council (NRC), Committee on Earthquake Engineering, Washington (1985)
28. Rangaswamy, R.; Boominathan, A.; Rajagopal, K.: Grain and specimen size effects on liquefaction of fine sands to undrained cyclic triaxial loading. In: Ayothiraman, R.; Hazarika, H. (eds.) Earthquake Hazards and Mitigation, pp. 423–430. I.K. Int. Pub. House Pvt. Ltd., New Delhi (2008)
29. Yilmaz, Y.; Mollamahmutoglu, M.: Characterisation of liquefaction susceptibility of sands by means of extreme void ratios and/or

void ratio range. J. Geotech. Geoenviron. Eng. **135**(12), 1986–1990 (2009)
30. Lee, K.L.; Albaisa, A.: Earthquake induced settlements in saturated sands. J. Geotech. Eng. Div. ASCE **100**(4), 387–406 (1974)
31. El Hosri, M.S.; Biarez, J.; Hicher, P.Y.: Liquefaction characteristics of silty clay. In: Proceedings of 8th World Conference Earthquake Engineering, vol. 3, pp. 277–284. San Francisco (1984)
32. Seed, H.B.; Martin, P.P.; Lysmer, J.: Pore water pressure change during soil liquefaction. J. Geotech. Eng. Div. ASCE **102**(4), 323–346 (1976)
33. Wang, J., Kavazanjian, E.: Pore-Water Pressure Development in Non-Uniform Cyclic Triaxial Tests. John A. Blume Earthquake Engineering Center Rep. No. 73, Technical Dept. of Civil and Environmental Engineering, Stanford Univ., Stanford (1985)
34. Polito, C.P.; Green, R.A.; Lee, J.: Pore pressure generation models for sands and silty soils subjected to cyclic loading. J. Geotech. Geoenviron. Eng. **134**(10), 1490–1500 (2008)
35. Menq, F.-Y.; Stokoe, II. K.H.: Linear dynamic properties of sandy and gravelly soils from large-scale resonant tests. In: Di Benedetto et al. (eds.) Deformation Characteristics of Geomaterials, Swets and Zeitlinger, Lisse, pp. 63–67 (2003)
36. Edil, T.B.; Luh, G.F.: Dynamic modulus and damping relationships for sands. In: Proceedings of ASCE Speciality Conference on Earthquake Engineering and Soil Dynamics, vol. 1, pp. 394–409 (1978)